FOREX Publication
Open Access | Rapid and quality publishing

International Journal of
Electrical and Electronics Research (IJEER)
Research Article | Volume 12, Issue 1 | Pages 28-35 | e-ISSN: 2347-470X

Accuracy Measurement of Hyperspectral Image Classification in Remote Sensing with the Light Spectrum-based Affinity Propagation Clustering-based Segmentation

A. Josephine Christilda[1*] and R. Manoharan[2]
[1]*Research Scholar, Sathyabama Institute of Science and Technology, Chennai - 600113, India; jchristilda@yahoo.com*
[2]*Assistant Professor, Sathyabama Institute of Science and Technology, Chennai - 600113, India; mano_rl@yahoo.co.in*

***Correspondence:** A. Josephine Christilda; jchristilda@yahoo.com

ABSTRACT- The area of remote sensing and computer vision includes the challenge of hyperspectral image classification. It entails grouping pixels in hyperspectral pictures into several classes according to their spectral signature. Hyperspectral photographs are helpful for a variety of applications, including vegetation study, mineral mapping, and mapping urban land use, since they include information on an object's reflectance in hundreds of small, contiguous wavelength bands. This task's objective is to correctly identify and categorize several item categories in the image. Many approaches have been stated by several researchers in this field to enhance the accuracy of the segmentation and accuracy. However, fails to attain the optimal accuracy due to the intricate nature of the images. To tackle these issues, we propose a novel Modified Extreme Learning machine (M-ELM) approach for the credible hyperspectral image classification outcomes with the publicly available Kaggle datasets. Before the classification, the input images are segmented using the Light Spectrum-based modified affinity propagation clustering technique (LSO-MAPC). In the beginning, the images are pre-processed using the non-linear diffusion partial differential equations technique which effectively pre-processed the image spatially. Experiments are effectuated to analyze the performance of the proposed method and compared it with state-of-art works in a quantitative way. The proposed approach ensures a classification accuracy of 96%.

Keywords: Hyperspectral images; Modified Extreme learning machine; Light spectrum optimization; Affinity propagation clustering.

ARTICLE INFORMATION

Author(s): A. Josephine Christilda and R. Manoharan;
Received: 31/10/2023; **Accepted**: 28/12/2023; **Published**: 20/01/2024;
e-ISSN: 2347-470X;
Paper Id: IJEER 3110-30;
Citation: 10.37391/IJEER.120105
Webpage-link:
https://ijeer.forexjournal.co.in/archive/volume-12/ijeer-120105.html

Publisher's Note: FOREX Publication stays neutral with regard to Jurisdictional claims in Published maps and institutional affiliations.

1. INTRODUCTION

Hyperspectral imaging (HSI) [1] technology examines a broad range of radiation, instead of only designating the three major colors (red, green, and each pixel. To offer additional details about the image depicted, the illumination impacting every molecule is divided into a variety of spectral ranges. Multispectral data [2] sets typically consist of 5 to 10 bands with very high frequencies (70-400 nm), while hyper-spectrum information collections often consist of 100 to 200 wavelengths with comparatively modest frequencies (5-10 nm). The whole wavelength range is collected and processed during hyperspectral image acquisition [3].

To locate things, recognize resources, or observe procedures imaging aims to get the wavelengths for every single bit in a picture of an object. Compared to multispectral data, data has better features for identifying and differentiating specific characteristics or entities. Due to their ability to acquire limited bandwidth knowledge, they can give comprehensive data regarding any item. Precise resolution of wavelengths is a feature of hyperspectral detectors. The atmosphere, distance, and undersea vehicles employ ultraviolet sensors to collect precise wavelength metrics for a variety of uses. It is easier to distinguish between various characteristics on the globe's surface when using indicators, which collect pictures in a large number of confined, continuous wavelengths.

In addition to synthetic aperture radar (SAR) [4] and traditional data, it is an additional information format. Contrary to multidimensional space missions, do not require radiation to provide light for their images. Sending repeated radio waves to light a target region, then listening for and collecting the bounces of each repetition results in the creation of a picture. It uses wavelengths with different frequencies that are not always connected, whereas imaging uses confined, often continuous optical bands [5] with potentially thousands or even hundreds of components. A condensed portion of the technique is what mapping is, the discipline of imaging and visual computing includes the challenge of image classification [6], which entails grouping pixel values in pictures into multiple categories according to their optical pattern.

The decomposition of the observed visual range of hyper-spectrum information into its component fingerprints and an assortment of matching proportionate quantities. It is increasingly used to track the growth and wellness of produce, despite the expense of capturing hyperspectral pictures often

FOREX Publication
Open Access | Rapid and quality publishing
International Journal of Electrical and Electronics Research (IJEER)
Research Article | Volume 12, Issue 1 | Pages 28-35 | e-ISSN: 2347-470X

being expensive for others and in certain regions. The development of a system to notify people early for outbreaks of illnesses and the use of scanning instrumentation to identify a specific variety are both ongoing projects. Image segmentation [7] is frequently used to identify boundaries and items in pictures, described in more exact terms, is the method of giving every molecule in a picture a name to ensure that objects with an identical tag have specific properties.

Segmenting wellness reasons and biological pictures using encoder-decoder designs: Among the two most often utilized structures for clinical and biological visualization are U-Net and V-Net [8], the primary use of U-Net is for the division of pictures from organic imaging. In context with these issues, we propose an innovative Modified Extreme Learning machine (M-ELM) approach for hyperspectral image classification and LSO-MAPC-based segmentation. Major contributions are,

- The proposed approach is to enhance the hyperspectral image classification accuracy with a lower error rate and therein significantly reduces the complexity.
- The images from the Kaggle dataset are pre-processed using the non-linear diffusion partial differential equation the spatially remove the noise and smoothen the images.
- The segmentation of the images is effectuated with the innovative Light spectrum optimization-based Modified Affinity Propagation clustering approach which improves the segmentation accuracy.
- The proposed Modified Extreme Learning machine (M-ELM) can be utilized to enhance the classification accuracy with a lower error rate.

The remainder of the work is arranged as follows: in *section 2* the existing work of hyperspectral image classification with their challenges and advantages. In *section 3* the proposed work is elucidated briefly. The experimental analysis is explained in *section 4*. The conclusion section is summarized in *section 5*.

2. LITERATURE SURVEY

Hong et al. [9] have presented graph convolutional networks (GCN) in the investigation and display of inconsistent information. The method constructs an enhancement of the current system to make them more suitable for the hyperspectral classification of images task after thoroughly analysing both networks from four distinct angles. A universal throughout its entirety merging system is produced by our final introduction of three distinct fusion algorithms. The suggested method is more adaptable in that it can forecast the fresh input data points, or the out-of-sample instances, without the network needing to be retrained. However, it is insufficient to establish more sophisticated fusion segments.

Hang et al. [10] have described an attention-aided Convolutional neural networks (CNN) model to categorize hyperspectral pictures spectrally and spatially. To acquire attributes, tiny cubes are often first cut from the hyperspectral picture and then input into the spectral-spatial method. The ability to discriminate between various spectral wavelengths and geographic positions within the cubes. If thoroughly examined, this past knowledge will aid in enhancing networks' potential for learning. It efficiently enhances the performance of the system. Nevertheless, it is challenging to fully investigate the inherent characteristics of information.

Zheng et al. [11] have implemented a fast patch-free global learning (FPGA) framework to classify hyperspectral images. To determine the significance of the attribute maps, monochromatic consideration includes modelling the mutual dependence of the map elements. This guarantees adequate use of the repetitive wavelength data and broad geographical data. With a lower priority on optimization, the identification pattern is gradually recovered using a portable coder. It would improve the rapidity and precision of spectral categorization. Thus, global optimization of the entire system and adequate use of global geographical information are not possible.

Liu et al. [12] have developed multitask deep learning technique in the open world (MDL4OW) that carries out categorization and restoration in the real environment concurrently. The rebuilt data gets contrasted to the source values; those that cannot be reconstituted are categorized as unidentified because designations prevent them from being accurately captured in the hidden qualities. To distinguish between the unidentified and identified classes, a level of significance must be established. The reliability of hyperspectral image categorization with unidentified classes is determined effectively. Still, it will be challenging to recognize the unclear divisions if the categorization method covers all fundamental land cover components.

Gao et al. [13] have demonstrated a multiscale residual network (MSRN) for the classification of spectral images. In contrast to those processes employing multiscale components, those using single-scale provides typically only perform multiscale feature mining once, making it difficult to fully understand the depiction of spectral-spatial features at various scales. Which can carry out multiscale feature extraction at different levels of the network. It can carry out multiscale feature extraction at different levels of the network. Thus, will also have an impact on the application effect that occurs.

Li et al. [14] have modified deep learning-based algorithms by eliminating inherent and conceptual properties, which are frequently used to categorize images. It is used to reduce the harm that noise and anomalies do, creating a deeper infrastructure that is more reliable and accurate. To be able to effectively extract valuable information from multisource information in classifying multisource sensor records. It designs a solid and reliable generalization model. Therefore, it has a poor representational ability since its inputs, as well as its outcomes, are both variables.

Liu et al. [15] suggested deep learning-based methods to improve the small sample classification performance of hyperspectral images. It is more applicable to the structural feature block in combination with multi-grained imaging. The complex network architecture, meanwhile, has been shown in multiple investigations to increase the precision of

FOREX Publication
Open Access | Rapid and quality publishing
International Journal of Electrical and Electronics Research (IJEER)
Research Article | Volume 12, Issue 1 | Pages 28-35 | e-ISSN: 2347-470X

classification. It is a quick and effective technique. However, need extensive hyperparameter changes.

Su et al. [16] highlighted tangent space collaborative representation classification (TCRC) has obtained exceptional hyperspectral image recognition efficiency in a condensed vector space. It is employed as a poor classifier; it is coupled to create a robust classifier. Despite taking longer to develop than independent classification systems, and group training outperforms them in terms of accuracy. Efficiency and precision can be achieved if the system is more responsive to the data used for training or variables. Thus, it causes a model's capacity to be understood to decline.

An efficient and effective semi-supervised spectral-spatial HSI classification method based on sparse superpixel graph (SSG) has been proposed [18]. In the constructed sparse superpixels graph, each vertex represents a superpixel instead of a pixel, which greatly reduces the size of graph. Meanwhile, both spectral information and spatial structure are considered by using superpixel, local spatial connection, and other methods. The authors of [17] introduce a novel taxonomy and group some existing methods into three groups: IS-based methods, ISE-PG-based methods, and ESE-KT-based methods. Compared with the existing reviews, the proposed novel taxonomy is more conducive to the extraction and analysis of method generalities, making the categories more distinct and distinguishable from each other.

3. PROPOSED METHODOLOGY

The proposed methodology is for the classification and detection of hyperspectral images and our approach is based on the Modified affinity propagation clustering (MAPC) based segmentation and a novel M-ELM for the classification of segmented hyperspectral images. Before these two phases, the images are spatially pre-processed using the non-linear diffusion partial differential equations. The overlay of the proposed approach is interpreted in *figure 1*.

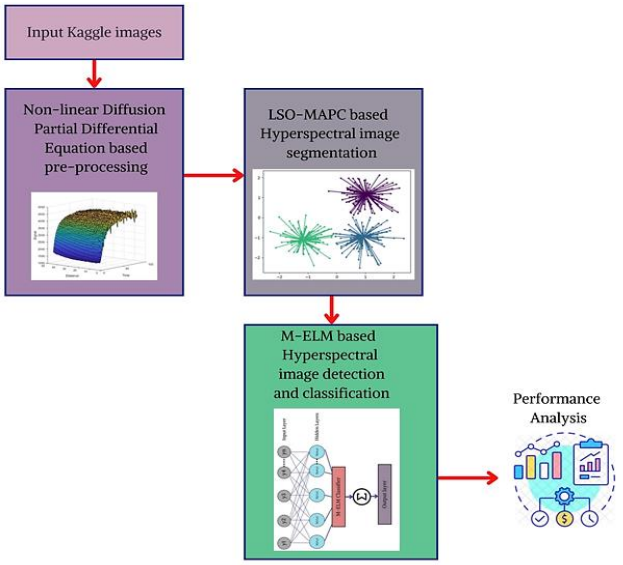

Figure 1: Overlay of proposed Hyperspectral image classification and detection

3.1 Pre-processing

In the hyperspectral images, the noises are removed using the spatial pre-processing approach which also smoothens the images. This approach often enhances the spatial texture information and therein significantly improves the classifier accuracy [19].

3.2 Modified Affinity Propagation Clustering (MAPC)

The proposed innovative MAPC is used for the segmentation of images taken. Previously, it is observed that the segmentation of images had improved the classification of HSI accuracy and a large generation of segmented regions might push the classification to predict wrongly. For this reason, we proposed a novel MAPC algorithm [20]. Utilizing the MAPC might be deemed the pixel of the images as a potential exemplar and created the sub-segments. The main reason for choosing the MAPC is that there is no need to determine the sub-segments earlier and it automatically chooses based on the specific issue. To begin the segmentation of the images the sub-segmented regions are created with the correlation among each pixel. The similarity index $SI(i,l)$ is measured for each pixel of k to determine the exact exemplar of pixel i. The measured Euclidean distance is not only responsible for the correlation of pixels but also easily determined in the search space. Hence, we have stated a negative Euclidean distance and henceforth, the similarity index $SI(i,l)$ can be formulated as follows,

$$SI(i,l) = -\|m_i - m_l\|^2 \quad (1)$$

The location of pixel i and j are determined as m_i and $m_l$respectively. After the completion of the similarity index of each pixel, the proposed approach utilizesthe message-passing technique. The data between two pixels are exchanged in two forms namely availability and responsibility. The steps involved in this are elucidated below,

At first, the initial value of the availabilities of the pixels $A(i,l)$ is regulated as 0 and followed by the measurement of responsibilities as $SI(i,l)$.

$$R(i,l) = SI(i,l) - max\{A(i,j) + SI(i,j)\}\, s.t.\, j \in \{1,2,3,\ldots,N\},\ j \neq l \quad (2)$$

The up-gradation of availabilities is effectuated as below,

$$A(i,l) = min\{0, R(l,l) + \textstyle\sum_{j\neq\{i,l\}} max\{0, R(j,l)\}\} \quad (3)$$

However, the measurement of self-availability is different from *eq. (3)* and it is outlined as follows [21],

$$A(l,l) = \textstyle\sum_{j\neq l} max\{0, R(j,l)\} \quad (4)$$

Moreover, the numerical oscillations during the damping can be averted with the consideration of the following means.

$$R(i,l) = \rho \times R(i,l)_{previous} + (1-\rho) \times R(i,l) \quad (5)$$

$$A(i,l) = \rho \times A(i,l)_{previous} + (1-\rho) \times A(i,l) \quad (6)$$

FOREX Publication
Open Access | Rapid and quality publishing
International Journal of Electrical and Electronics Research (IJEER)
Research Article | Volume 12, Issue 1 | Pages 28-35 | e-ISSN: 2347-470X

The damping factor is determined as ρ which lies on the interval of 0 and 1. Subsequently, the pixel l can be considered as an exemplar if l=*i*. The aforementioned procedure follows until the measured exemplar got unchanged for more than two iterations. Thus, the segmentation of hyperspectral images is formed automatically with the proposed MAPC.

3.3 Light Spectrum Optimizer (LSO)

The metrological phenomenon inspires the Light Spectrum Optimizer (LSO). The assumptions are depending upon LSO such as (i) Candidate solutions are represented using every colorful ray, (ii) The ranges from 40o to 42o is the light ray's dispersion, (iii) The global best solution is the light ray's population that reaches so far to the best dispersion, (iv) Randomly control the reflection and refraction and (v) Comparing to best so far fitness solution, initial phases with the rainbow colors curves are managed via the fitness of current solutions. LSO mathematical representation is outlined below;

3.3.1 Initialization

For the initialization of white random light are started using the LSO search process [22].

$$\overrightarrow{y^0} = B_L + PU_1(B_U - B_L) \quad (7)$$

A random vector PU_1 uniformly moves to the ranges [0, 1] with the initial solution $\overrightarrow{y^0}$. Where d is the dimension of a problem with upper and lower bounds are B_U and B_L.

3.3.2. Light rays based on the dispersion of various colors

The LSO exportation, exploitation, scattering of colourful rays, and the direction of the rainbow spectrum are the mechanism as follows;

3.3.2.1 Rainbow spectrum direction

The below formulas explain the normal vectors of outer refraction, inner reflection, and inner refraction are given as,

$\vec{y}_{mD}$, $\vec{y}_{mB}$ and $\vec{y}_{mA}$.

$$\vec{y}_{mD} = \frac{\overrightarrow{y^*}}{Nor\left(\overrightarrow{y^*}\right)} \quad (8)$$

$$\vec{y}_{mB} = \frac{\overrightarrow{y_t^r}}{Nor\left(\overrightarrow{y_t^r}\right)} \quad (9)$$

$$\vec{y}_{mA} = \frac{\overrightarrow{y_t^p}}{Nor\left(\overrightarrow{y_t^p}\right)} \quad (10)$$

At iteration t, the solution randomly selected is $\overrightarrow{y_t^p}$ and the current solution is $\overrightarrow{y_t^r}$. Find the global solution is $\overrightarrow{y^*}$ with $Nor(\cdot)$ represents the vector normalized value. The below expression computes the vector normalized value.

$$Nor\left(\vec{y}\right) = \sqrt{\sum_{k=0}^{D} y_k^2} \quad (11)$$

The dimension is D with the input vector $\vec{y}$. This formula measures the incident light ray.

$$\overrightarrow{y_{L0}} = \frac{Y_{mean}}{Nor(Y_{mean})} \quad (12)$$

The current population means is Y_{mean} with the solution $\overrightarrow{y_j}$ $(j = 1, \ldots, M)$. The population size is M with $\overrightarrow{y_{L0}}$ the incident light ray.

3.3.2.2 Exploration scheme (Create new colorful ray)

Randomly create the probability r of solutions ranges [0, 1]. Equation (13) computes the new solution candidates.

$$\vec{y}_{T+1} = \vec{y}_T + \delta PU_1^m\left(\vec{y}_{L1} - \vec{y}_{L3}\right) \times \left(\vec{y}_{p1} - \vec{y}_{p3}\right) \quad (13)$$

Create the new candidate solution and the current solutions around $\vec{y}_T$. Uniform random vectors around PU_2^m. The scaling factor is δ.

3.3.2.3 Exploitation scheme (Scattering or colorful rays)

The exploitation operator is improved with the current population with the chosen solution.

$$\vec{y}_{T+1} = \vec{y}_T + PU_3\left(\vec{y}_{p1} - \vec{y}_{p2}\right) + PU_4^m \times (P < \alpha) \times \left(\vec{y}^* - \vec{y}_T\right) \quad (14)$$

The current solution and the best so far solution to the new position.

$$\vec{y}_{T+1} = 2\,cos(\pi \times p_1)\left(\overrightarrow{y^*}\right)\left(\overrightarrow{y_T}\right) \quad (15)$$

3.4 LSO-MAPC-based Segmentation of hyperspectral images

The proposed LSO-MAPC utilizes an exclusion scheme and convergence predictions are effectuated for the optimal allocation of computing resources for the segmented images. The former is used to avert the overlapping issues that occur while performing the clustering process and the latter process assist to stagnate the segmented images that are converged.

3.5 Proposed Modified Extreme Learning Machine (M-ELM) based Hyperspectral image classification

The hyperspectral image classification is effectuating with the utilization of our proposed robust approach known as M-ELM [24]. The main use of M-ELM is that it prevents the initialization procedures followed in input and hidden layers. The proposed schematic is illustrated in *figure 2*. Considered m number of samples in the training dataset taken as (y_t, v_t) with the hidden layers of h for our approach. The activation function of the proposed M-ELM is formulated as,

$$\sum_{t=1}^{h} \beta_t a(y_t) = \sum_{t=1}^{h} \beta_t a(z_t . y_t + e_t) = v_o where, o = 1,2,3,\ldots t \quad (16)$$

Subsequently, the output of the M-ELM is

FOREX Publication
Open Access | Rapid and quality publishing
International Journal of Electrical and Electronics Research (IJEER)
Research Article | Volume 12, Issue 1 | Pages 28-35 | e-ISSN: 2347-470X

$$K_h(y) = \sum_{t=1}^{h} \delta_t \, a(z_t . y + e_t) = \lambda . h(y) \quad (17)$$

The weight vectors that are interconnected with the input and t^{th} hidden neuron arez_t, and the hidden neuron interlinked with the output are taken as β_t. The hidden layer output is implied concerning the input y and the bias of the t^{th} hidden neurona_t. Meanwhile, the initiated hidden neurons are much lower than the overall training instances and thus created the non-square matrix with the parameter S [23, 24]. With this condition the$\beta$is unavailable, however, it is ineluctable to compute the value for measurement of the output neuron's weight.

$$\delta = S^{*}W \quad (18)$$

For our proposed approach the measured value using $S^{*}$is an essential need and is represented as Moore-Penrose generalized inverse utilized for the matrix S. Subsequently, the positive value $\frac{1}{\vartheta}$is appended to the ELM as the kernel value while measuring the β value as shown,

$$\beta = S^{P}\left(\frac{1}{\vartheta} + SS^{P}\right)^{-1} w \quad (19)$$

Here, $w$is the user-defined value, and the feature mapping in the hidden layer is performed to reveal the kernel function of the ELM. The kernel function of ELM is implied as q and is formulated as,

$$q_{ELM} = SS^{P} : q_{ELMt,o} = h(y_t).h(y_o) = C(y_t, y_o) \quad (20)$$

Here the kernel function is taken as $C(y_t, y_o)$ and its respective output is,

$$\begin{bmatrix} C(y,y1) \\ . \\ . \\ . \\ C(y,y_o) \end{bmatrix}^{P} \left(\frac{1}{\vartheta} + q_{ELM}\right)^{-1} W \quad (21)$$

For the proposed M-ELM several kernel functions used here are tangent, Gaussian, and wavelet functions. The soft plush parameter of ELM is interpreted as,

$$sp(y) = log(1 + f^{y}) \quad (22)$$

For the improvement of hyperspectral classification accuracy our proposed approach is utilized with the mitigation of the error rate. Accuracy is also enhanced with the reduction of complexity of the procedures that are followed.

The proposed M-ELM is used to train and test the images from the dataset that are originally selected. The proposed approach handles the classification pixel-wise and also determines the pixel-wise classification map. Moreover, the proposed approach also detects the super pixels based on the segmentation performed by the proposed innovative LSO-MAPC approach. This ensures the classification of hyperspectral images based on the category and attains higher classification accuracy.

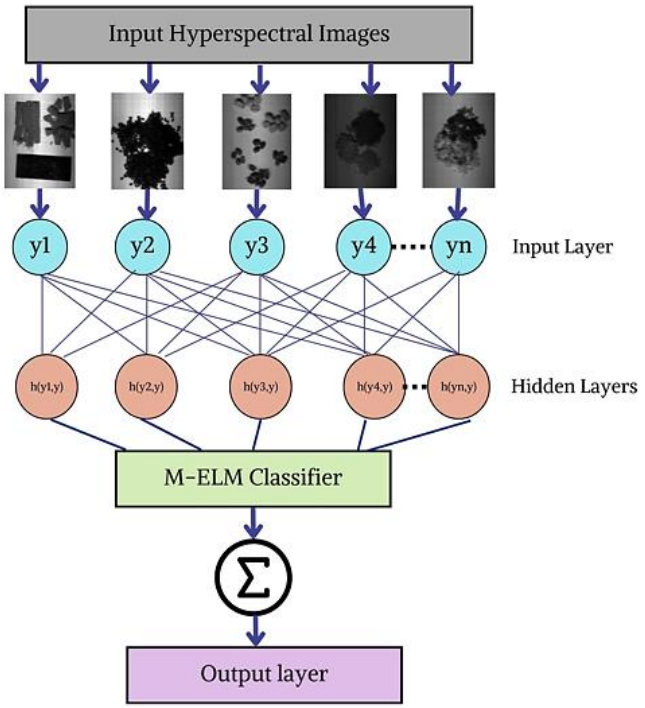

Figure 2: The framework of M-ELM used for the classification of hyperspectral images

4. RESULT AND DISCUSSION

The implementation platform of Python investigates the experimental outcomes related to proposed hyperspectral image segmentation and classification. The effectiveness of the proposed hyperspectral image categorization method was measured overall using statistical parameters. The population size of LSO is 100 with the maximum number of iterations is 1being.

4.1 Dataset Description

Dataset images for this study are collected from the Kaggle dataset (https://www.kaggle.com/c/ipsa-ma511/data). There are 103 spectral bands with 310 x 340 pixels present in the dataset to train hyperspectral images. The train_y.npy determines the respective image label. *Figure 3* tabulates the hyperspectral classification results in which the classified objects are differentiated using various kinds of colors.

Ground truth image	Classified hyperspectral image
	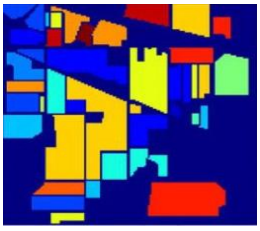

FOREX Publication
Open Access | Rapid and quality publishing
International Journal of Electrical and Electronics Research (IJEER)
Research Article | Volume 12, Issue 1 | Pages 28-35 | e-ISSN: 2347-470X

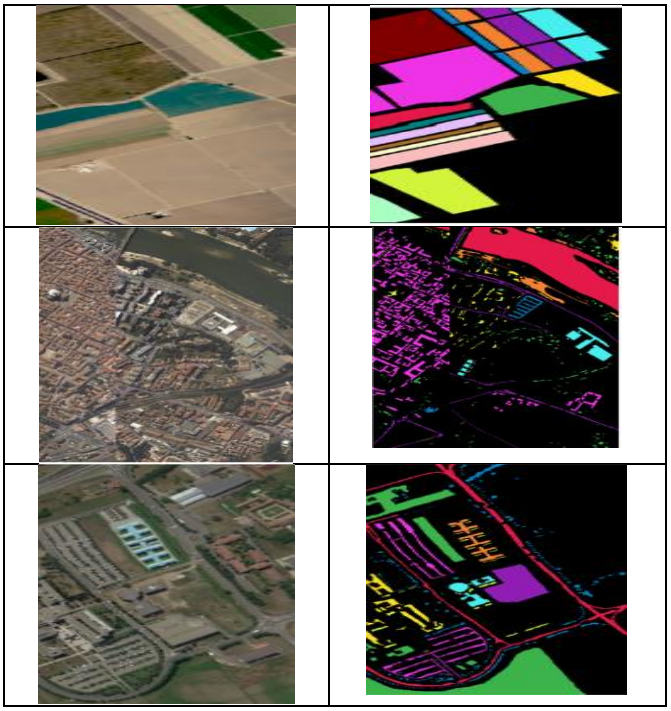

Figure 3: Hyperspectral classification

4.2 Evaluation Measures

Various evaluation measures are taken here to check the efficiency of the proposed framework using statistical parameters like structural similarity index (SSIM) accuracy (A), sensitivity (Sen), specificity (Spec), Mathew's Correlation Coefficient (MCC), and so on to check the capability of proposed techniques in terms of both segmentation and classification.

The hyperspectral image segmentation is measured as,
Structural Similarity Index (SSIM):

Structural Similarity Index measures the similarity between two images. It ranges from -1 to 1, where 1 indicates a perfect match.

$$SSIM = \frac{(2a_\beta b_\alpha + c_1)(\sigma_{ab} + c_2)}{(a_\alpha^2 + b_\alpha^2 + c_1)(a_\alpha^2 + b_\alpha^2 + c_2)} \quad (23)$$

The mean values of images are a_β and b_α. The constant values are c_1 and c_2.

$$A = \frac{T^{-ve} + T^{+ve}}{T^{-ve} + F^{-ve} + T^{+ve} + F^{+ve}} \quad (24)$$

$$Spec = \frac{T^{-ve}}{T^{-ve} + F^{+ve}} \quad (25)$$

$$Sen = \frac{T^{+ve}}{T^{+ve} + F^{-ve}} \quad (26)$$

$$MCC = \frac{\left((T^{+ve} * T^{-ve}) - (F^{+ve} - F^{-ve})\right)}{\sqrt{(T^{+ve} + F^{+ve})((T^{+ve} + F^{-ve})(T^{-ve} + F^{+ve})(T^{-ve} + F^{-ve}))}} \quad (27)$$

By this equation, the truly positive and negative predicted classes are T^{+ve} and T^{-ve}. As well as, F^{+ve} and F^{-ve} are the false positive and negative classes. These metrics provide different aspects of the segmentation performance. SSIM gives an indication of the similarity between the segmented image and the ground truth. Accuracy provides an overall correctness measure, Sensitivity and Specificity give insights into the performance on positive and negative instances, and MCC is a balanced metric that considers all four confusion matrix values.

4.3 Performance Investigation

The state-of-art result of SSIM is illustrated in Figure 4. State-of-art approaches like GCN [9], CNN [10], FPGA [11], MSRN [13], and proposed methods are used to check the hyperspectral image segmentation from SSIM. Regarding the methodologies GCN [9], CNN [10], FPGA [11], and MSRN [13], the proposed framework outperformed an SSIM result of 88%, 90%, 88%, 84%, and 95%. This plot demonstrates that the proposed work surpassed the existing techniques in terms of SSIM results.

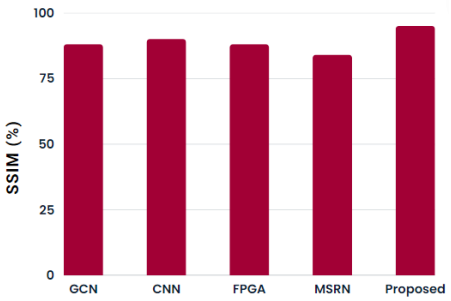

Figure 4: Comparative study for SSIM results

The comparative study for the number of iteration Vs accuracy is illustrated in *figure 5*. *Figure 6* shows the comparison analysis for the number of iterations vs. specificity.

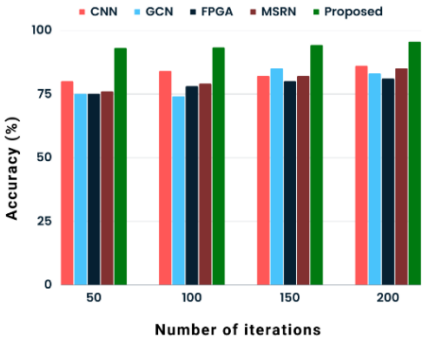

Figure 5: Comparative study for the number of iteration Vs accuracy

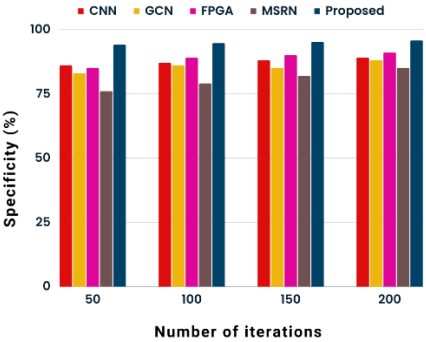

Figure 6: Comparative study for the number of iteration Vs specificity

FOREX Publication
Open Access | Rapid and quality publishing
International Journal of Electrical and Electronics Research (IJEER)
Research Article | Volume 12, Issue 1 | Pages 28-35 | e-ISSN: 2347-470X

The comparison study for iterations Vs sensitivity is shown in *figure 7*. *Table 1* illustrates the computational time comparison. Investigating the outcome of computational time is covered by existing methods like GCN [9], CNN [10], FPGA [11], and MSRN [13] with the proposed approach. In comparison to other methods like GCN [9], CNN [10], FPGA [11], and MSRN [13], the proposed methodology required less computing time to complete the task.

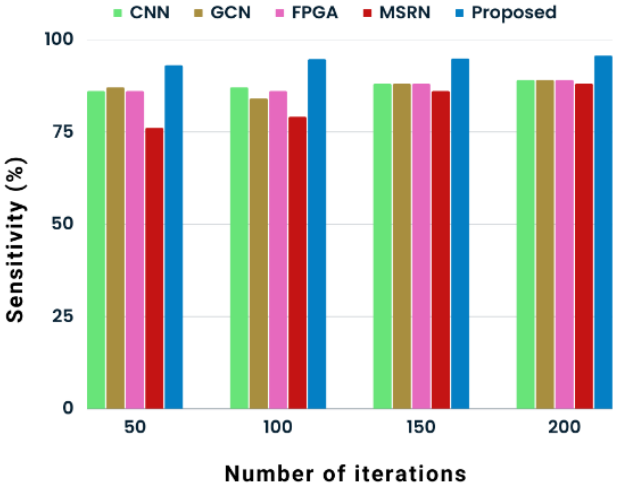

Figure 7: Comparative study for the number of iteration Vs sensitivity

Table 1. Comparison of computational time

Methods	Time in seconds (s)
GCN [9]	6.5s
CNN [10]	8.4s
FPGA [11]	7.32s
MSRN [13]	10.32s
Proposed approach	2.12s

Figure 8 plots the comparative study for the number of iterations Vs MCC. The effectiveness of current approaches such as GCN [9], CNN [10], FPGA [11], MSRN [13], and proposed methods are used to show the MCC of hyperspectral categorization. Regarding the number of iterations, the proposed method outperformed MCC levels of 93%, 94.63%, 94.78%, and 95.56%. The proposed system overtook the previous GCN [9], CNN [10], FPGA [11], and MSRN [13] techniques in terms of MCC. The robustness of Light Spectrum-based Affinity Propagation Clustering-based Segmentation is a multifaceted aspect that depends on the interplay of data characteristics, parameter choices, and the specific demands of the application. Careful consideration of these factors, along with thorough validation and testing, is essential to assess and improve the robustness of the segmentation approach in practice.

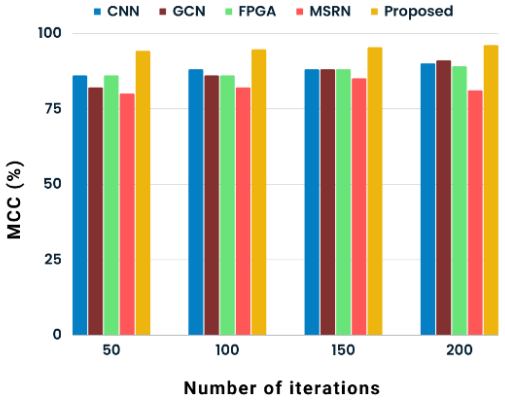

Figure 8: Comparative study for the number of iterations Vs MCC

5. CONCLUSION

This paper presented a novel modified extreme learning machine-based hyperspectral image classification. Dataset images are gathered from publicly available Kaggle datasets that are implemented using Python software. SSIM, accuracy, sensitivity, specificity, and MCC are used as the evaluation parameters in experiments to statistically analyze the effectiveness of the proposed approach and compare it to existing approaches. The result of the proposed work outlined 95% SSIM, 96% accuracy, 95.67% specificity, 95.56% sensitivity, and 95.56% MCC to compare with the previous techniques such as GCN, CNN, FPGA, and MSRN. While analysing computational time, this work offers a minimum of 2.12s time.

Author Contributions

The authors confirm contribution to the paper as follows: study conception and design: A. Josephine Christilda, R. Manoharan; data collection: A. Josephine Christilda; analysis and interpretation of results: R. Manoharan; draft manuscript preparation: A. Josephine Christilda All authors reviewed the results and approved the final version of the manuscript.

Acknowledgments

The authors would like to thank the reviewers for all of their careful, constructive and insightful comments in relation to this work.

Conflicts of Interest

The authors declare that they have no known competing financial interests or personal relationships that could have appeared to influence the work reported in this paper.

REFERENCES

[1] Lei, J.; Li, X.; Peng, B.; Fang, L.; Ling, N.; Huang, Q. Deep spatial-spectral subspace clustering for hyperspectral image. IEEE Transactions on Circuits and Systems for Video Technology 2020, Volume 31, No. 7, pp. 2686-2697.

[2] Xie, Q.; Zhou, M.; Zhao, Q.; Xu, Z.; Meng, D. MHF-Net: An interpretable deep network for multispectral and hyperspectral image fusion. IEEE Transactions on Pattern Analysis and Machine Intelligence 2020, Volume 44, No. 3, pp. 1457-1473.

[3] Lin, H.Y.; Liang, S.C.; Chen, Y.K. Robotic grasping with multi-view image acquisition and model-based pose estimation. IEEE Sensors Journal 2020, Volume 21, No. 10, pp. 11870-11878.

FOREX Publication
Open Access | Rapid and quality publishing

International Journal of
Electrical and Electronics Research (IJEER)
Research Article | Volume 12, Issue 1 | Pages 28-35 | e-ISSN: 2347-470X

[4] Saju, Chinju, Parwin Angel Michael, Jarin. T. Hybrid electric car comparison to increase the reliability for fuel efficiency. Renewable Energy Focus 2022, Volume 43, pp. 309-316.

[5] Galdino, L.; Edwards, A.; Yi, W.; Sillekens, E.; Wakayama, Y.; Gerard, T.; Pelouch, W.S.; Barnes, S.; Tsuritani, T.; Killey, R.I.; Lavery, D. Optical fibre capacity optimisation via continuous bandwidth amplification and geometric shaping. IEEE Photonics Technology Letters 2020, Volume 32, No. 17, pp. 1021-1024.

[6] Ramana, T. V.; Pandian, A.; Ellammal, C.; Jarin, T.; Ahmed Nabih Zaki Rashed, Sampathkumar. A. Numerical analysis of circularly polarized modes in coreless photonic crystal fiber. Results Phys 2019, Volume 13, No. 102140, pp. 10-1016.

[7] Sinha, A.; Dolz, J. Multi-scale self-guided attention for medical image segmentation. IEEE journal of biomedical and health informatics 2020, Volume 25, No. 1, pp. 121-130.

[8] El Jurdi, R.; Petitjean, C.; Honeine, P.; Abdallah, F. Bb-unet: U-net with bounding box prior. IEEE Journal of Selected Topics in Signal Processing 2020, Volume 14, No. 6, pp. 1189-1198.

[9] Hong, D.; Gao, L.; Yao, J.; Zhang, B.; Plaza, A.; Chanussot, J. Graph convolutional networks for hyperspectral image classification. IEEE Transactions on Geoscience and Remote Sensing 2020, Volume 59, No. 7, pp. 5966-5978.

[10] Hang, R.; Li, Z.; Liu, Q.; Ghamisi, P.; Bhattacharyya, S.S. Hyperspectral image classification with attention-aided CNNs. IEEE Transactions on Geoscience and Remote Sensing 2020, Volume 59, No. 3, pp. 2281-2293.

[11] Zheng, Z.; Zhong, Y.; Ma, A.; Zhang, L. FPGA: Fast patch-free global learning framework for fully end-to-end hyperspectral image classification. IEEE Transactions on Geoscience and Remote Sensing 2020, Volume 58, No. 8, pp. 5612-5626.

[12] Liu, S.; Shi, Q.; Zhang, L. Few-shot hyperspectral image classification with unknown classes using multitask deep learning. IEEE Transactions on Geoscience and Remote Sensing 2020, Volume 59, No. 6, pp. 5085-5102.

[13] Gao, H.; Yang, Y.; Li, C.; Gao, L.; Zhang, B. Multiscale residual network with mixed depthwise convolution for hyperspectral image classification. IEEE Transactions on Geoscience and Remote Sensing 2020, Volume 59, No. 4, pp. 3396-3408.

[14] Li, H.C.; Wang, W.Y.; Pan, L.; Li, W.; Du, Q.; Tao, R. Robust capsule network based on maximum correntropy criterion for hyperspectral image classification. IEEE Journal of Selected Topics in Applied Earth Observations and Remote Sensing 2020, Volume 13, pp. 738-751.

[15] Liu, B.; Guo, W.; Chen, X.; Gao, K.; Zuo, X.; Wang, R.; Yu, A. Morphological attribute profile cube and deep random forest for small sample classification of hyperspectral image. IEEE Access 2020, Volume 8, pp. 117096-117108.

[16] Su, H.; Yu, Y.; Du, Q.; Du, P. Ensemble learning for hyperspectral image classification using tangent collaborative representation. IEEE Transactions on Geoscience and Remote Sensing 2020, Volume 58, No. 6, pp. 3778-3790.

[17] Wang, X.; Liu, J.; Chi, W.; Wang, W.; Ni, Y. Advances in Hyperspectral Image Classification Methods with Small Samples: A Review. Remote Sens. 2023, No. 15, pp. 3795.

[18] Zhao, Y.; Yan, F. Hyperspectral Image Classification Based on Sparse Superpixel Graph. Remote Sens. 2021, 13, pp. 3592.

[19] Goez, M.M.; Torres-Madronero, M.C.; Rothlisberger, S.; Delgado-Trejos, E. Joint pre-processing framework for two-dimensional gel electrophoresis images based on nonlinear filtering, background correction, and normalization techniques. BMC bioinformatics 2020, Volume 21, No. 1, pp. 1-16.

[20] Zhang, J.; He, M.; Dai, Y. Modified affinity propagation clustering. In 2014 IEEE China Summit & International Conference on Signal and Information Processing (ChinaSIP) 2014, July, pp. 505-509. IEEE.

[21] Serdah, A.M.; Ashour, W.M. Clustering large-scale data based on modified affinity propagation algorithm. Journal of Artificial Intelligence and Soft Computing Research 2016, Volume 6, No. 1, pp. 23-33.

[22] Abdel-Basset, M.; Mohamed, R.; Sallam, K.M.; Chakrabortty, R.K. Light spectrum optimizer: a novel physics-inspired metaheuristic optimization algorithm. Mathematics 2022, Volume 10, No. 19, pp. 3466.

[23] Priya, M.; Vijay. M. M. Error detection and correction for SRAM systems using improved redundant matrix code. In 2019 International Conference on Recent Advances in Energy-efficient Computing and Communication (ICRAECC) 2019, pp. 1-8. IEEE.

[24] Yin, H.; Dong, Z.; Chen, Y.; Ge, J.; Lai, L.L.; Vaccaro, A.; Meng, A. An effective secondary decomposition approach for wind power forecasting using extreme learning machine trained by crisscross optimization. Energy conversion and management 2017, Volume 150, pp. 108-121.